

Controllable Non-Hermitian Qubit-Qubit Coupling in Superconducting Quantum Circuit

Hui Wang,^{1, 2, *} Yan-Jun Zhao,³ and Xun-Wei Xu^{4, †}

¹*Inspur artificial intelligence research institute, Jinan, 250014, China*

²*Shandong Yunhai Guochuang Innovative Technology Co., Ltd., Jinan 250101, China*

³*Key Laboratory of Opto-electronic Technology, Ministry of Education,
Beijing University of Technology, Beijing, 100124, China*

⁴*Key Laboratory of Low-Dimensional Quantum Structures and Quantum Control of Ministry of Education,
Key Laboratory for Matter Microstructure and Function of Hunan Province,
Department of Physics and Synergetic Innovation Center for Quantum Effects and Applications,
Hunan Normal University, Changsha 410081, China*

(Dated: April 11, 2024)

With a high-loss resonator supplying the non-Hermiticity, we study the energy level degeneracy and quantum state evolution in the tunable coupling superconducting quantum circuit. The qubits' effective energy levels and damping rates can be continually tuned by the qubit-resonator coupling phase and amplitude, quantum states of qubits, and effective qubit-qubit coupling strength, thus the positions and numbers of level degenerate points are controllable. The efficient of quantum state exchange and the asymmetry of quantum state evolution can be tuned with non-hermitian and nonreciprocal coupling between two qubits. The controllable non-Hermiticity provides new insights and methods for exploring the unconventional quantum effects in superconducting quantum circuit.

I. INTRODUCTION

Non-Hermitian system possessing complex energy spectrum, the corresponding real and imaginary parts respectively label the energy levels and loss, and the degenerate point of energy levels are known as the exceptional points[1–5]. The system close to exceptional points contain rich unconventional physical effects, including the ultralow driving threshold chaos[29], high sensitivity metrology[7, 8], high-dimensions skin effect[9, 10], chiral heat transport[11] and so on. The exceptional point have been studied in single ion system[12, 13], optical microcavity[14–21], and optomechanical system[22–25], magnonic system[26–28], hybrid quantum system[29], single superconducting qubit[30, 31], and so on. Some theoretical work have studied the \mathcal{PT} -symmetry in superconducting circuit with the single qubit coupling to the resonator[32, 33]. However, it is still challenging to experimentally observe such non-Hermitian in multi-qubits superconducting circuit due to the difficulties in realizing controlled gain and loss.

Unlike the efforts to improve the gain and loss of superconducting resonator, we use a high-loss resonator supplying the effective non-hermitian interactions between two qubits in tunable coupling superconducting circuit. Using the advantage of easy tuning for superconducting artificial atoms, the energy level degenerate and exceptional points of the non-Hermitian superconducting circuit are controlled by the phases and amplitudes of qubit-resonator coupling, the effective qubit-qubit coupling, and the quantum state of qubits. Because of special parameter dependent relation in tunable coupling

superconducting circuit, we find that the energy level degenerate point can be one or a series in different parameter regimes, and the positions of the exceptional points are controllable. The forward and backward coupling between two qubits are still non-reciprocal in non-Hermitian superconducting circuit, which can be used to develop the integrated unidirectional transmission devices.

By preparing one qubit in the excited state and another in the ground states, the free evolution of quantum states under non-Hermite interaction can be tuned with the resonator-qubit coupling phases. Even setting the identical parameters, the evolutions of two qubits' quantum states are different from different coupling directions. The non-reciprocal couplings in superconducting circuit can be used to develop the integrated unidirectional transmission devices including the microwave circulator and isolator.

The paper is organized as follows: In Sec. II, we build the model of non-Hermitian superconducting circuit; In Sec. III, the energy level degeneracy and the quantum state evolution are tuned in energy level attraction regimes; In Sec. IV, we analyze the non-reciprocal coupling and asymmetric quantum state evolutions. We finally summarize the results in Sec. V.

II. EFFECTIVE NON-HERMITIAN CIRCUIT

As shown in Fig. 1, we study a superconducting circuit consisting of two Xmon qubits coupling to a common transmon coupler and a high-loss superconducting resonator. The transmon coupler and the high-loss resonator can induce the hermite and non-hermite indirect interaction between two qubits. The free Hamiltonian for the superconducting circuit can be written as

* wanghuiphy@126.com

† xwxu@hunnu.edu.cn

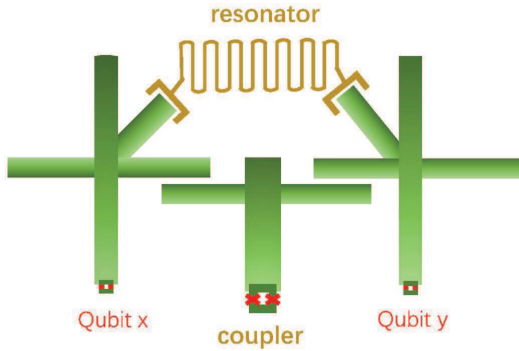


FIG. 1. (Color online) The superconducting circuit consisting of two Xmon qubits coupling to a common transmon coupler and a high-loss resonator. The capacitance type interaction is dominated in the superconducting circuit.

$H_0 = \omega_a a^\dagger a + \sum_{k=1,2,c} (\omega_k/2) \sigma_z^{(k)}$. ω_a is the resonant frequency of resonator, and the corresponding transition frequency of superconducting artificial atoms are defined as ω_k , where $k = 1, 2, c$ label the qubit 1, qubit 2, and the transmon coupler, respectively. a^\dagger and a are the creation and annihilation operators for the resonator photons, and $\sigma_z^{(k)}$ is the Pauli-Z operator of artificial atom. The Hamiltonian for the direct qubit-qubit interaction is $H_{xy} = g_{xy} [\sigma_+^{(1)} \sigma_-^{(2)} + \sigma_+^{(2)} \sigma_-^{(1)}]$, where g_{xy} label the direct coupling strength between two qubits. We define the $\sigma_\pm^{(k)}$ as the ladder operators of artificial atoms. The Hamiltonian for the interaction between coupler and qubit- j can be written as $H_{qc}^j = g_j [\sigma_+^{(c)} \sigma_-^{(j)} + \sigma_+^{(j)} \sigma_-^{(c)}]$, where g_j is the coupling strength between qubit- j and transmon coupler, with $j = 1, 2$.

In this article, the frequency detuning microwave is applied on qubit to create amplitude and phase tunable J-C interaction between qubit and resonator[34–36]. The qubits and resonator are in the dispersive coupling regimes, that is $\lambda_j^{(0)} \ll |\Delta_{ja}|, |\Delta_{ja} + \alpha_j|$, where $\lambda_j^{(0)}$ labels the bare resonator-qubit coupling amplitude between first-excited state of superconducting artificial atom- j and the fundamental mode of resonator and their frequency detuning is $\Delta_{ja} = \omega_j - \omega_a$, while α_j describe the anharmonicity of qubit- j . After injecting a single tone microwave pulse with amplitude $\Omega_j(t)$ and phase $\theta_j(t)$, thus resonator-qubit- j interaction can be obtained as $\lambda_j \exp(\theta_j)$, with $\lambda_j = (1/\sqrt{2}) \lambda_j^{(0)} \alpha_j |\Omega_j| / [\Delta_{ja}(\Delta_{ja} + \alpha_j)]$ [34, 35]. The amplitude λ_j and phase θ_j can be tuned by the input microwave pulse, thus the Hamiltonian for amplitude and phase tunable resonator-qubit coupling can be written as $H_{qr}^j = [\lambda_j \exp(-i\theta_j) a^\dagger \sigma_-^{(j)} + \lambda_j \exp(i\theta_j) \sigma_+^{(j)} a]$. The interaction between resonator and transmon coupler is very weak and can be neglected, thus the Hamiltonian for the superconducting circuit in Fig. 1 can be obtained as $H = H_0 + H_{xy} + \sum_j H_{qc}^j + \sum_j H_{qr}^j$.

In the weak dispersive coupling regimes $g_j/|\Delta_{jc}| \sim 1/3$

(with $\Delta_{jc} = \omega_j - \omega_c$), the Schrieffer-Wolff transformation $U = \exp \sum_{j=1,2} (g_j/\Delta_{jc}) [\sigma_+^{(c)} \sigma_-^{(j)} - \sigma_+^{(j)} \sigma_-^{(c)}]$ can be applied to Hamiltonian H to cancel the qubit-coupler interaction terms[37, 38]. Thus the effective Hamiltonian of two qubits coupling to a common high-loss resonator can be written as

$$\begin{aligned} \frac{H'}{\hbar} = & \omega_a a^\dagger a + \left(\omega_j + \sum_{j=1,2} \frac{g_j^2}{\Delta_{jc}} \right) \frac{\sigma_z^{(j)}}{2} \\ & + g_e \left[\sigma_+^{(1)} \sigma_-^{(2)} + \sigma_+^{(2)} \sigma_-^{(1)} \right] \\ & + \sum_{j=1,2} \lambda_j \left[\exp(-i\theta_j) a^\dagger \sigma_-^{(j)} + \exp(i\theta_j) \sigma_+^{(j)} a \right], \end{aligned} \quad (1)$$

where the subscripts $j = 1, 2$ label the qubit 1 and qubit 2, respectively. The effective interaction between two qubits is defined as $g_e = g_{xy} + g_1 g_2 / \Delta_e$ with $2/\Delta_e = 1/\Delta_{1c} + 1/\Delta_{2c}$, where the first term is the direct qubit-qubit interaction and the second term labels the indirect interaction induced by the transmon coupler[39–41]. The indirect qubit-qubit interaction induced by the high-loss resonator is the non-hermite type and not contained in g_e . Since $g_{xy} \ll g_j$, the invariance assumption is made for H_{xy} during the Schrieffer-Wolff transformation, and the tunable coupler is assumed as the ground states and thus the free Hamiltonian of transmon coupler is neglected.

In the rotating coordinates at resonator's frequency ω_a , the motion equations of cavity photon and qubit- j can be written as $\dot{a} = -\gamma_a a - i \sum_{j=1,2} \lambda_j \exp(-i\theta_j) \sigma_-^{(j)}$ and $\dot{\sigma}_-^{(j)} = -[\gamma_j/2 + i(\Delta_{ja} + g_j^2/\Delta_{jc})] \sigma_-^{(j)} - i\lambda_j \exp(i\theta_j) \sigma_z^{(j)} a - i g_e \sigma_z^{(j)} \sigma_-^{(j+1)}$, with $\Delta_{ja} = \omega_j - \omega_a$ and $j+1=1$ for $j=2$. In the case of $\gamma_a \gg g_j, \lambda_j \gg \gamma_j$ and $|\Delta_{ja}|/\gamma_a \approx 1/3$, with the adiabatic approximation, we can get $a = -i(\lambda_1/\gamma_a) \sum_{j=1,2} \lambda_j \exp(-i\theta_j) \sigma_-^{(j)}$. Substituting it into the motion equation of ladder operators, thus we get

$$\begin{aligned} \dot{\sigma}_-^{(j)} = & - \left[\left(\frac{\gamma_j}{2} + \frac{\lambda_j^2}{\gamma_a} \sigma_z^{(j)} \right) + i \left(\Delta_{ja} + \frac{g_j^2}{\Delta_{jc}} \right) \right] \sigma_-^{(j)} \\ & - \left[i g_e + \frac{\lambda_j \lambda_{j+1}}{\gamma_a} \exp[i(\theta_j - \theta_{j+1})] \right] \sigma_z^{(j)} \sigma_-^{(j+1)}. \end{aligned} \quad (2)$$

The Pauli-Z operator $\sigma_z^{(j)}$ describes the population of qubit- j and its steady value can be tuned with external microwave signals. Though coupling to a high-loss resonator, the decoherence time of qubit should be much longer than the operation times (usually below 100 ns) for preparation and readout of single qubit's quantum states especially for the tantalum-based superconducting qubit[42, 43]. Thus the population of qubit- j can be considered as staying in the transient stability value $\langle \sigma_z^{(j)} \rangle$ during the measurement for the quantum state of single qubit, and its value can be tuned by the qubit-coupler coupling strength, and also the resonator-qubit coupling

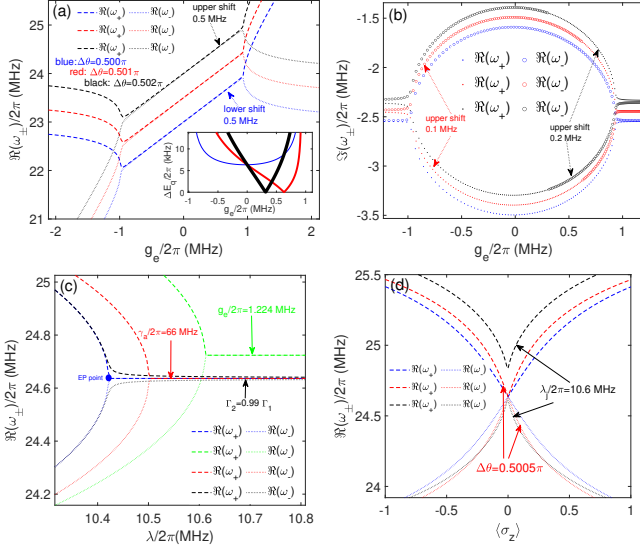


FIG. 2. (Color online) Controllable levels degeneracy in non-hermitian superconducting circuit. (a) Effective energy levels and (b) damping rates as the function of effective coupling g_e . The three colored curves correspond to the phase differences: $\Delta\theta = 0.500\pi$ (blue curves), 0.501π (red curves), and 0.502π (black curves). The two qubits are assumed in the ground states $\langle\sigma_z^j\rangle = -1$, with $j = 1, 2$. (c) Effective energy levels as the function of resonator-qubit coupling amplitude λ_j . The four colored curves correspond to different parameters: $\Delta\theta = 0.500\pi$, $\Gamma_2 = \Gamma_1$, $g_e/2\pi = 1.137$ MHz, and $\gamma_a/2\pi = 65$ MHz (blue curves); $g_e/2\pi = 1.224$ MHz (green curves); $\gamma_a/2\pi = 66$ MHz (red curves); $\Gamma_2 = 0.99\Gamma_1$ (black curves). $\langle\sigma_z^{(1)}\rangle = -1$, and the un-mentioned parameters in the green, red, and black curves are the same as in blue curves. (d) Effective energy levels as function of qubits' populations $\langle\sigma_z^j\rangle$. The three colored curves correspond to different parameters: $\Delta\theta = 0.500\pi$, $\lambda_j/2\pi = 11$ MHz, $g_e/2\pi = 1.137$ MHz (blue curves); $\Delta\theta = 0.5005\pi$, $g_e/2\pi = 1.224$ MHz, $\lambda_j/2\pi = 11$ MHz (black curves). $\langle\sigma_z^j\rangle = (-1)^{(j+1)}\langle\sigma_z\rangle$, the un-mentioned parameters in the red and black curves are the same as in blue curves. The other parameters in (a)-(d) are: $\omega_a/2\pi = 4.475$ GHz, $\omega_1/2\pi = 4.5$ GHz, $\omega_2/2\pi = 4.505$ GHz, $\omega_c^{(max)}/2\pi = 5.20$ GHz, $\gamma_1/2\pi = 1.00$ MHz, $\gamma_2/2\pi = 1.01$ MHz, $g_{xy}/2\pi = 4.0$ MHz, $\lambda_j/2\pi = 11$ MHz, $g_1/2\pi = 30$ MHz, $g_2/2\pi = 30.3$ MHz, and $\gamma_a/2\pi = 65$ MHz.

phases and amplitudes. Thus the effective Hamiltonian for non-Hermitian qubit-qubit coupling can be written as

$$\frac{H''}{\hbar} = \begin{pmatrix} \frac{1}{2}(\Delta'_{1a} - i\Gamma_1) & g_e - \frac{i\lambda_1\lambda_2}{\gamma_a} \exp(i\Delta\theta) \\ g_e - \frac{i\lambda_1\lambda_2}{\gamma_a} \exp(-i\Delta\theta) & \frac{1}{2}(\Delta'_{2a} - i\Gamma_2) \end{pmatrix}, \quad (3)$$

where $\Delta\theta = \theta_1 - \theta_2$, $\Delta'_{ja} = \Delta_{ja} + g_j^2/\Delta_{jc}$, and $\Gamma_j = \gamma_j - \lambda_j^2 \langle\sigma_z^{(j)}\rangle/\gamma_a$, with $j = 1, 2$. The non-diagonal terms in Eq.(3) label total effective qubit-qubit coupling strength in the non-hermitian superconducting circuit. The two Eigen-modes of H'' can be calculated as

$$\omega_{\pm} = \frac{\Delta'_{1a} + \Delta'_{2a}}{4} - i\frac{\Gamma_1 + \Gamma_2}{4} \pm \sqrt{R + iI}, \quad (4)$$

with

$$R = \frac{(\Delta'_{1a} - \Delta'_{2a})^2}{4} - \frac{(\Gamma_1 - \Gamma_2)^2}{4} + 4g_e^2 - \frac{4\lambda_1^2\lambda_2^2}{\gamma_a^2}, \quad (5)$$

$$I = -\frac{8g_e\lambda_1\lambda_2}{\gamma_a} \cos(\Delta\theta) - \frac{(\Gamma_1 - \Gamma_2)(\Delta'_{1a} - \Delta'_{2a})}{2}. \quad (6)$$

The real parts $\Re(\omega_{\pm})$ and imaginary parts $\Im(\omega_{\pm})$ describe the effective energy levels and effective damping rates of two qubits, respectively. The values of R and I affect the separations of complex energy spectrum between two Eigen-modes, and the signs of R decide the level repulsions or attractions, while the sign of I describes the relative size of two effective damping rates.

III. CONTROLLABLE NON-HERMITIAN COUPLING

The experimental tunable parameters in this article include the resonator-qubit coupling phase and amplitude, effective qubit-qubit coupling, and occupation populations of qubits. If the parameters is tuned to satisfy $R < 0$ and $I = 0$, thus the $\sqrt{R + iI}$ becomes a pure imaginary number($\Delta E_q = 0$), and the energy levels of two qubits merge as one and the exceptional point appears. Even for a tiny nonzero value for I , the energy levels of two qubits will misalign and the exceptional point should be absent[25].

By setting two qubits in the ground states, the effective energy levels and damping rates of two Eigen-modes as the function effective qubit-qubit coupling (g_e) are shown in Figs. 2(a) and 2(b), respectively. The separations of two qubits' effective energy levels (or damping rates) becomes narrower (or wider) in certain parameter regimes corresponding to the the energy level attraction. To see clearer, the curves in blue and black color shift up -0.5 MHz or 0.5 MHz in Fig. 2(a), respectively. In the case of $\Delta\theta = \pi/2$, the first term in the right side of Eq.(6) is always zero, since $\Delta'_{1a} - \Delta'_{2a} \neq 0$ in parameter area of drawing, so there is no level degenerate point on the blue color curves in Fig. 2(a) and the insert figure. For $\Delta\theta \neq \pi/2$, as the variations of g_c (or ω_c), it is possible to satisfy $I = 0$ so the level degenerate points appear on the pairs of two red or black color curves. The scattering curves for damping rates of two qubits are shown in Fig. 2(b), to see clearer, the red and black color curves shift up 0.1 MHz and 0.2 MHz, respectively. The two branch of effective damping rates exchange with each other in two red or black color curves, and the corresponding exchange positions coincide well with those of level degenerate points in Fig. 2(a), which indicate the positions of exceptional points.

The effects of resonator-qubit coupling amplitudes on energy levels of two qubit are studied in Fig. 2(c). In the case of $\Delta\theta = \pi/2$ and $\Gamma_1 - \Gamma_2 = 0$, the first and second terms in Eq.(6) are always zeroes, so the energy level degeneracy appear for arbitrary value of λ_j (energy level

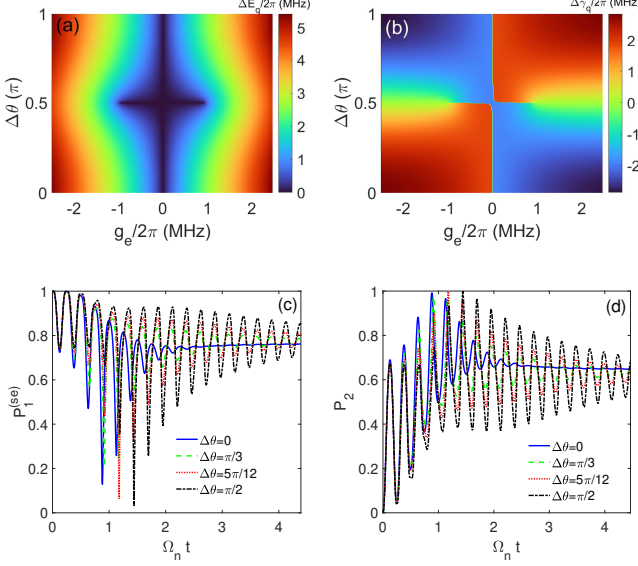


FIG. 3. (Color online) Controllable quantum state evolutions in energy level attraction regimes. (a) The energy level difference (ΔE_q) and (b) damping rate difference ($\Delta \gamma_q$) as functions of phase difference ($\Delta \theta$) and coupling strength (g_e). The two qubits are assumed as in the ground states, $\langle \sigma_z^{(j)} \rangle = -1$ with $j = 1, 2$. The evolutions of qubits' excited state occupation probabilities for (c) qubit 1 and (d) qubit 2. The four colored curves correspond to different phase differences: $\Delta \theta = 0$ (blue-solid curves); $\Delta \theta = \pi/3$ (green-dashed curves); $\Delta \theta = 5\pi/12$ (red-dotted curves); $\Delta \theta = \pi/2$ (black-dash-dotted curves). The qubit 1 and qubit 2 respectively start in excited and ground states. A small effective coupling ($g_e/2\pi = -80$ kHz) is chosen for energy level attractions in (c) and (d). The other parameters of four images are: $\omega_a/2\pi = 4.475$ GHz, $\omega_1/2\pi = 4.5$ GHz, $\omega_2/2\pi = 4.505$ GHz, $\omega_c^{(max)}/2\pi = 5.20$ GHz, $\gamma_1/2\pi = 1.00$ MHz, $\gamma_2/2\pi = 1.01$ MHz, $g_{xy}/2\pi = 4.0$ MHz, $\lambda_j/2\pi = 11$ MHz, $g_1/2\pi = 30$ MHz, $g_2/2\pi = 30.3$ MHz, and $\gamma_a/2\pi = 65$ MHz.

attraction regimes) in the blue curves. The change for the values of g_e can shift the position of the Exception point and also the value of energy levels as indicated by the green curves (compared with the blue curves). If the $\Gamma_1 - \Gamma_2 \neq 0$, because of no solution for $\Delta'_{1a} - \Delta'_{2a} \neq 0$ in the parameter area of drawing, so the energy level degenerate points does not appear in the red and black curves. As indicated by the motion equation of $\sigma_z^{(j)}$, the effective energy levels of two qubits can be tuned by changing the quantum states of qubits.

The value of $\Gamma_1 - \Gamma_2$ depends on the populations $\langle \sigma_z^{(j)} \rangle$ of qubit- j , and the energy level degenerate point can appear when the quantum states of qubits satisfy $\Gamma_1 - \Gamma_2 = 0$ as indicated by the blue ($\Delta \theta = \pi/2$) and red-dashed ($\Delta \theta = 0.5005\pi$) curves. Since the $\Delta'_{1a} - \Delta'_{2a} \neq 0$ in the parameter area of drawing and the first term of Eq.(6) is zero in the case of $\Delta \theta = \pi/2$, so the $I = 0$ can not be satisfied in the parameter regimes of $\Gamma_1 - \Gamma_2 \neq 0$ and there is no energy level degenerate points in the

black-dashed curve. To change the transient value of $\langle \sigma_z^{(j)} \rangle$, the qubit- j should be firstly initialized to the ground states and then excited to a new quantum states with the microwave pulses.

The separations between two effective energy levels and two damping rates of Eigen-modes can be defined as $\Delta E_q = \Re \omega_+ - \Re \omega_- = 2\Re(\sqrt{R+iI})$ and $\Delta \gamma_q = \Im \omega_+ - \Im \omega_- \approx 2\Im(\sqrt{R+iI})$, respectively. In the case of $\langle \sigma_z^{(j)} \rangle = -1$ ($\Gamma_1 - \Gamma_2 \neq 0$), the differences in energy levels (ΔE_q) and in damping rates ($\Delta \gamma_q$) as the function of effective coupling strength g_e and phase difference $\Delta \theta$ are plotted in Figs. 3(a) and 3(b), respectively. In the parameter regimes of small values for $\Delta'_{1a} - \Delta'_{2a}$, $\Gamma_1 - \Gamma_2$, and $\lambda_1 \lambda_2 / \gamma_a^2$, the value of R is smaller for weaker effective coupling g_e according to Eq.(5), and the value of I is close to zero in the case of $\cos \Delta \theta \approx 0$. Thus the levels difference ΔE_q gets local minimal values close to the regimes of $g_e \rightarrow 0$ or $\Delta \theta \rightarrow \pi/2$ in Fig. 3(a). The sign of I decides the relative size of two effective damping rates, thus the sign of $\Delta \gamma_q$ changes between two sides of the line $g_e \approx 0$ or $\Delta \theta \approx \pi/2$ in Fig. 3(b). The exceptional points can be found at the parameter regimes close $\Delta E_q \rightarrow 0$ and $\Delta \gamma_q \rightarrow 0$ in Figs. 3(a) and 3(b).

The free evolutions of quantum states under non-hermitian coupling can be calculated with the semiclassical limit method by disregarding the quantum jump terms[31, 47, 48]. By preparing the qubit 1 in the excited states and qubit 2 in the ground states, the time evolution of occupation probabilities for qubits' excited state can be calculated with the semiclassical master equation $\dot{\rho} = -i(H''\rho - \rho H'')$, where the ρ is the density operator. To stay in the level attraction regimes, the effective qubit-qubit coupling g_e is tuned to a small value, $g_e/2\pi = -80$ kHz. The time evolution of occupation probabilities for qubit-1 ($P_1^{(se)}$) starting in excited state and qubit-2 ($P_2^{(sg)}$) starting in ground state are shown in Fig. 3(c) and Fig. 3(d), respectively. The periodic oscillation of the curves originates from the nonzero frequency detuning Δ_{ja} in H'' , and the effects of the resonator-qubit coupling phase can be reflected by the variation of the envelopes.

The larger oscillating amplitudes in the black-dash-dotted curves for $\Delta \theta \approx \pi/2$ originates from the small damping rate contributed by non-hermite coupling close to exceptional points. The maximal amplitude of non-hermite coupling strength is defined as $\Omega_n = \lambda_1 \lambda_2 / \gamma_a$, the positions of local maximal or minimal values for the envelope are different on the four curves which originate from the dependencies of total qubit-qubit coupling on the phase difference $\Delta \theta$. The different values of local maximal values on envelope imply that the efficient of quantum state exchange between two qubits can be tuned by the resonator-qubit coupling phase, and the exchange efficient gets the highest value close to the exception point. In the black curves ($\Delta \theta = \pi/2$), the envelope of occupation probability drops slowly compared with the results on the blue-solid ($\Delta \theta = 0$), green-dashed

($\Delta\theta = \pi/3$), and red dash-dotted ($\Delta\theta = 5\pi/12$) curves, which indicates the different contributions of the non-hermite coupling on the effective damping rates of qubits. The quantum state exchange efficient and the costing time getting local maximal values can be tuned with the resonator-qubit coupling phases which might be useful to enhance the speed and fidelity of two-qubit quantum gates.

IV. NONRECIPROCAL COUPLING

The non-reciprocal coupling and photon transmission can also be realized in non-Hermitian system[44–47, 50, 51]. According to Eq.(3), the non-Hermitian coupling strengths between two qubits in the forward and backward directions can be respectively defined as $g_{1\leftarrow 2}^{(q)} = g_e - i\Omega_n \exp(\mp i\Delta\theta)$, and the first and second term label the Hermite and non-Hermite type qubit-qubit coupling, respectively.

The $g_{1\rightarrow 2}^{(q)} \neq g_{1\leftarrow 2}^{(q)}$ even in the case of $\Delta\theta = n\pi$ and the local maximal (or minimal) values of $|g_{1\rightarrow 2}^{(q)}|$ and $|g_{1\leftarrow 2}^{(q)}|$ are out of steps as shown in Figs. 4(a) and 4(b), which implies the non-reciprocal coupling for two different directions of effective qubit-qubit coupling. The minimal values of $|g_{1\rightarrow 2}^{(q)}|$ and $|g_{1\leftarrow 2}^{(q)}|$ could reach zero in Fig. 4(e) for $\Delta\theta = \pi/2$, but they get nonzero minimal value in the case of $\Delta\theta = \pi/3$ in Fig. 4(c). And the nonreciprocal ratio is much stronger in the case of $\Delta\theta = \pi/2$ as indicated by the maximal and minimal values of $|g_{1\leftarrow 2}|/|g_{1\rightarrow 2}|$ in Figs. 4(d) and 4(f). The non-reciprocal coupling strengths between two qubits can also be tuned by the resonator-qubit coupling amplitudes and qubits' quantum states.

The nonreciprocal coupling between two qubits might result in the asymmetry of quantum state evolutions for different directions, which can be seen from the nonzero values of occupation probability difference for two qubits' excited states with the same initial states in Figs. 4(g) and 4(h). Beside the apparently asymmetric of occupation probabilities after the period $t > 1/\Omega_n$, the non-reciprocity of qubit quantum state evolution can also be tuned by the resonator-qubit coupling phases. Even adopting the same frequencies, same coupling strengths, same damping rates, and same initial states, the time evolution of qubit occupation probabilities from two different directions still do not overlap in Figs. 4(g) and 4(h), which coincides with the results of non-reciprocal coupling in Figs. 4(c) and 4(f).

V. CONCLUSIONS

In conclusion, the energy level degeneracies and quantum state evolutions are studied in non-Hermitian superconducting circuit. The efficient and asymmetry of quantum state evolutions can be tuned by the resonator-qubit

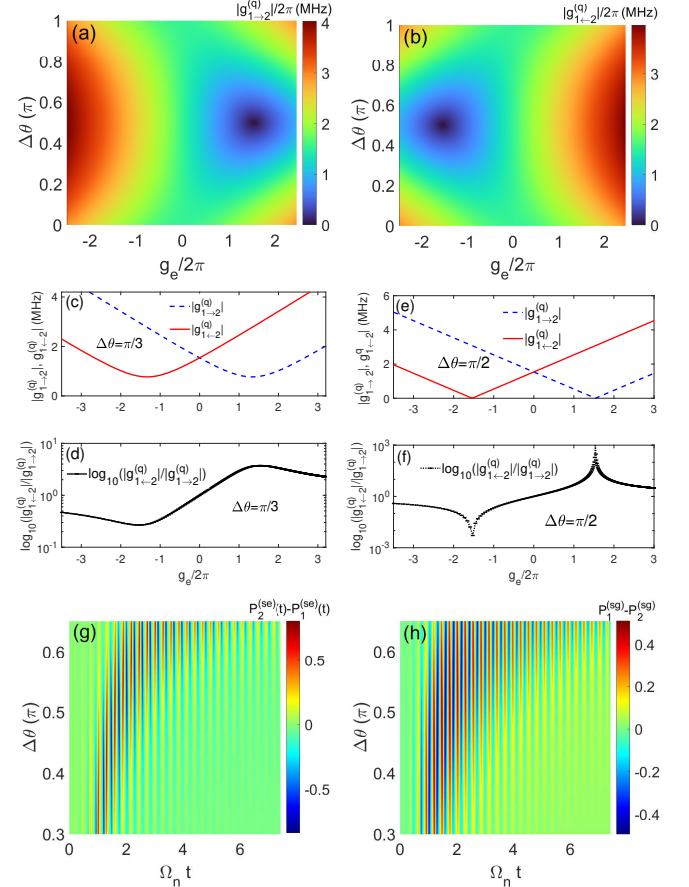


FIG. 4. (Color online) Controllable non-reciprocal couplings and state evolutions in non-Hermitian superconducting circuit. (a) Non-Hermitian coupling strengths $g_{1\rightarrow 2}^{(q)}$ and (b) $g_{1\leftarrow 2}^{(q)}$ as functions of phase difference $\Delta\theta$ and coupling strength g_e . The one-dimensional curves of $g_{1\rightarrow 2}^{(q)}$ (blue-dashed curve) and $g_{1\leftarrow 2}^{(q)}$ (red-solid curve) for (c) $\Delta\theta = \pi/3$ and (e) $\Delta\theta = \pi/2$. The non-reciprocal ratio $|g_{1\leftarrow 2}^{(q)}|/|g_{1\rightarrow 2}^{(q)}|$ for (d) $\Delta\theta = \pi/2$ and (f) $\Delta\theta = \pi/3$. The two qubits are assumed as in the ground states, $\langle\sigma_z^{(j)}\rangle = -1$ with $j = 1, 2$. The other parameters in (a)-(d) are: $\omega_a/2\pi = 4.475$ GHz, $\omega_1/2\pi = 4.5$ GHz, $\omega_2/2\pi = 4.505$ GHz, $\omega_c^{(max)}/2\pi = 5.20$ GHz, $\gamma_1/2\pi = 1.00$ MHz, $\gamma_2/2\pi = 1.01$ MHz, $g_{xy}/2\pi = 4.0$ MHz, $\lambda_j/2\pi = 11$ MHz, $g_1/2\pi = 30$ MHz, $g_2/2\pi = 30.3$ MHz, $g_e/2\pi = 1.137$ MHz, and $\gamma_a/2\pi = 65$ MHz. The differences in occupation probabilities of two qubits starting in (g) excited states ($P_j^{(ee)}$) and (h) ground ($P_j^{(gg)}$) states. $\omega_j/2\pi = 4.5$ GHz, $g_j/2\pi = 30$ MHz, and $\gamma_j/2\pi = 1$ MHz, with $j = 1, 2$, and the other parameters are the same as in (a)-(f) except for $g_e/2\pi \approx -80$ kHz.

coupling phase which might be useful for enhancing the fidelity and speeding of quantum gates. The resonator and qubits are in weak dispersive coupling regimes, so the state leakages and crosstalks are inevitable which should be suppressed with tunable coupler and wave-shape correction techniques[40].

VI. ACKNOWLEDGMENTS

We thanks Zhiguang Yan for useful discussions.. H.W. is supported by the Natural Science Foundation of Shandong Province under Grant No. ZR2023LZH002 and the Inspur artificial intelligence research institute. Y.J.Z. is supported by Beijing Natural Science Foundation under

Grant No. 4222064 and NSFC under Grant No. 11904013. X.-W.X. is supported by the National Natural Science Foundation of China (Grants No. 12064010 and No. 12247105), the Science and Technology Innovation Program of Hunan Province (Grant No. 2022RC1203), Natural Science Foundation of Hunan Province of China (Grant No. 2021JJ20036), and Hunan provincial major sci-tech program (Grant No. 2023ZJ1010).

[1] C.M. Bender, S. Boettcher, and P.N. Meisinger, PT-symmetric quantum mechanics, *J. Math. Phys.* **40**, 2201 (1999).

[2] C.M. Bender, D.C. Brody, and H.F. Jones, Complex extension of quantum mechanics, *Phys. Rev. Lett.* **89**, 270401 (2002).

[3] G. Lévai and M. Znojil, Systematic search for PT-symmetric potentials with real energy spectra, *J. Phys. Math. Gen.* **33**, 7165 (2000).

[4] C.M. Bender and S. Boettcher, Real Spectra in Non-Hermitian Hamiltonians Having PT Symmetry, *Phys. Rev. Lett.* **80**, 5243 (1998).

[5] R. El-Ganainy, K.G. Makris, M. Khajavikhan, Z.H. Musslimani, S. Rotter, and D. N. Christodoulides, Non-Hermitian physics and PT symmetry, *Nat. Phys.* **14**, 11 (2018).

[6] Xin-You Lü, Hui Jing, Jin-Yong Ma, and Ying Wu, PT-Symmetry-Breaking Chaos in Optomechanics, *Phys. Rev. Lett.* **114**, 253601 (2015).

[7] Weijian Chen, S.K. Özdemir, Guangming Zhao, J. Wiersig, and Lan Yang, Exceptional points enhance sensing in an optical microcavity, *Nature* **548**, 192 (2017).

[8] Zhong-Peng Liu, Jing Zhang, S.K. Özdemir, Bo Peng, Hui Jing, Xin-You Lü, Chun-Wen Li, Lan Yang, F. Nori, and Yu-xi Liu, PT-Symmetric Cavities: Enhanced Sensitivity near the PT-Phase Transition, *Phys. Rev. Lett.* **117**, 110802 (2016).

[9] Kai Zhang, Zhesen Yang, and Chen Fang, Universal non-Hermitian skin effect in two and higher dimensions, *Nat. Comm.* **13**, 2496 (2022).

[10] Yaohua Li, Chao Liang, Chenyang Wang, Cuicui Lu, and Yong-Chun Liu, Gain-Loss-Induced Hybrid Skin-Topological Effect, *Phys. Rev. Lett.* **128**, 223903 (2022).

[11] Guoqiang Xu, Xue Zhou, Ying Li, Qitao Cao, Weijin Chen, Yunfeng Xiao, Lan Yang, and Cheng-Wei Qiu, Non-Hermitian Chiral Heat Transport, *Phys. Rev. Lett.* **130**, 266303 (2023).

[12] Liangyu Ding, Kaiye Shi, Qiuxin Zhang, Danna Shen, Xiang Zhang, and Wei Zhang, Experimental Determination of PT-Symmetric Exceptional Points in a Single Trapped Ion, *Phys. Rev. Lett.* **126**, 083604 (2021).

[13] Wei-Chen Wang, Yan-Li Zhou, Hui-Lai Zhang, Jie Zhang, Man-Chao Zhang, Yi Xie, Chun-Wang Wu, Ting Chen, Bao-Quan Ou, Wei Wu, Hui Jing, and Ping-Xing Chen, Observation of PT-symmetric quantum coherence in a single-ion system, *Phys. Rev. A* **103**, L020201 (2021).

[14] B. Peng, S.K. Özdemir, F. Lei, F. Monifi, M. Giannfreda, G. L. Long, S. Fan, F. Nori, C. M. Bender, and L. Yang, Parity-timesymmetric whispering-gallery microcavities, *Nat. Phys.* **10**, 394 (2014).

[15] L. Chang, X. Jiang, S. Hua, C. Yang, J. Wen, L. Jiang, G. Li, G. Wang, and M. Xiao, Parity-time symmetry and variable optical isolation in active-passive-coupled microresonators, *Nat. Photonics* **8**, 524 (2014).

[16] L. Feng, Z. J. Wong, R.-M. Ma, Y. Wang, and X. Zhang, Single mode laser by parity-time symmetry breaking, *Science* **346**, 972 (2014).

[17] H. Hodaei, M.-A. Miri, M. Heinrich, D.N. Christodoulides, and M. Khajavikhan, Parity-time-symmetric microring lasers, *Science* **346**, 975 (2014).

[18] H. Hodaei, A.U. Hassan, S. Wittek, H. Garcia-Gracia, R. El-Ganainy, D. N. Christodoulides, and M. Khajavikhan, Enhanced sensitivity at higher-order exceptional points, *Nature (London)* **548**, 187 (2017).

[19] W. Chen, S.K. Özdemir, G. Zhao, J. Wiersig, and L. Yang, Exceptional points enhance sensing in an optical microcavity, *Nature (London)* **548**, 192 (2017).

[20] A.A. Zyablovsky, A.P. Vinogradov, A.A. Pukhov, A.V. Dorofeenko, and A.A. Lisynsky, PT-symmetry in optics, *Phys. Usp.* **57**, 1063 (2014).

[21] Huilai Zhang, Ran Huang, Sheng-Dian Zhang, Ying Li, Cheng-Wei Qiu, F. Nori, and Hui Jing, Breaking Anti-PT Symmetry by Spinning a Resonator, *Nano Lett.* **20**, 7594 (2020).

[22] H. Xu, D. Mason, Luyao Jiang, and J.G.E. Harris, Topological energy transfer in an optomechanical system with exceptional points, *Nature* **537**, 80 (2016).

[23] N. Wu, K. Cui, Q. Xu, X. Feng, F. Liu, W. Zhang, and Y. Huang, On-chip mechanical exceptional points based on an optomechanical zipper cavity, *Science Advances*, **9**, eabp8892 (2023).

[24] Cheng Jiang, Yu-Long Liu, and M.A. Sillanpää, Energy-level attraction and heating-resistant cooling of mechanical resonators with exceptional points, *Phys. Rev. A* **104**, 013502 (2021).

[25] N.R. Bernier, L.D. Tóth, A.K. Feofanov, and T.J. Kippenberg, Level attraction in a microwave optomechanical circuit, *Phys. Rev. A* **98**, 023841 (2018).

[26] H. Liu, D. Sun, C. Zhang, M. Groesbeck, R. McLaughlin, and Z. V. Vardeny, Observation of exceptional points in magnonic parity-time symmetry devices, *Sci. Adv.* **5**, eaax9144 (2019).

[27] Xi-guang Wang, Lu-lu Zeng, Guang-hua Guo, and J. Berakdar, Floquet Engineering the Exceptional Points in Parity-Time-Symmetric Magnonics, *Phys. Rev. Lett.* **131**, 186705 (2023).

[28] A.V. Sadovnikov, A.A. Zyablovsky, A.V. Dorofeenko, and S.A. Nikitov, Exceptional-Point Phase Transition in Coupled Magnonic Waveguides, *Phys. Rev. Applied* **18**, 024073 (2022).

[29] Guo-Qiang Zhang, Zhen Chen, Da Xu, N. Shammah, Meiyong Liao, Tie-Fu Li, Limin Tong, Shi-Yao Zhu, Franco Nori, and J. Q. You, Exceptional Point and Cross-Relaxation Effect in a Hybrid Quantum System, *PRX Quantum* **2**, 020307 (2021).

[30] F.F. Sani, I.C. Rodrigues, D. Bothner, and G.A. Steele, Level attraction and idler resonance in a strongly driven Josephson cavity, *Phys. Rev. Research* **3**, 043111 (2021).

[31] Weijian Chen, M. Abbasi, Y.N. Joglekar, and K.W. Murch, Quantum Jumps in the Non-Hermitian Dynamics of a Superconducting Qubit, *Phys. Rev. Lett.* **127**, 140504 (2021).

[32] G.A. Starkov, M.V. Fistul, and I.M. Eremin, Schrieffer-Wolff transformation for non-Hermitian systems: Application for PT-symmetric circuit QED, *Phys. Rev. B* **108**, 235417 (2023).

[33] F. Quijandría, U. Naether, S.K. Özdemir, F. Nori, and D. Zueco, PT-symmetric circuit QED, *Phys. Rev. A* **97**, 053846 (2018).

[34] S. Zeytinoğlu, M. Pechal, S. Berger, A.A. Abdumalikov, Jr., A. Wallraff, and S. Filipp, Microwave-induced amplitude- and phase-tunable qubit-resonator coupling in circuit quantum electrodynamics, *Phys. Rev. A* **91**, 043846 (2015).

[35] M. Pechal, L. Huthmacher, C. Eichler, S. Zeytinoğlu, A.A. Abdumalikov, Jr., S. Berger, A. Wallraff, and S. Filipp, Microwave-Controlled Generation of Shaped Single Photons in Circuit Quantum Electrodynamics, *Phys. Rev. X* **4**, 041010 (2014).

[36] P. Magnard, P. Kurpiers, B. Royer, T. Walter, J.-C. Besse, S. Gasparinetti, M. Pechal, J. Heinsoo, S. Storz, A. Blais, and A. Wallraff, Fast and Unconditional All-Microwave Reset of a Superconducting Qubit, *Phys. Rev. Lett.* **121**, 060502 (2018).

[37] S. Bravyi, D.P. DiVincenzo, and D. Loss, Schrieffer-wolff transformation for quantum many-body systems, *Annals of physics* **326**, 2793 (2011).

[38] S. Richer, Perturbative analysis of two-qubit gates on transmon qubits, thesis, (2013).

[39] F. Yan, P. Krantz, Y. Sung, M. Kjaergaard, D.L. Campbell, T. P. Orlando, S. Gustavsson, and W. D. Oliver, Tunable Coupling Scheme for Implementing High-Fidelity Two-qubit Gates, *Phys. Rev. Applied* **10**, 054062 (2018).

[40] Y. Sung, L. Ding, J. Braumüller, A. Vepsäläinen, B. Kannan, M. Kjaergaard, A. Greene, G.O. Samach, C. McNally, D. Kim, A. Melville, B.M. Niedzielski, M.E. Schwartz, J.L. Yoder, T.P. Orlando, S. Gustavsson, and W.D. Oliver, Realization of High-Fidelity CZ and ZZ-Free iSWAP Gates with a Tunable Coupler, *Phys. Rev. X* **11**, 021058 (2021).

[41] Hui Wang, Yan-Jun Zhao, Hui-Chen Sun, Xun-Wei Xu, Yong Li, Yarui Zheng, Qiang Liu, and Rengang Li, Controlling the qubit-qubit coupling in the superconducting circuit with double-resonator couplers, *Phys. Rev. A* **109**, 012601 (2024).

[42] A.P.M. Place, L.V.H. Rodgers, P. Mundada, B.M. Smitham, M. Fitzpatrick, Zhaoqi Leng, A. Premkumar, J. Bryon, A. Vrajitoarea, S. Sussman, Guangming Cheng, T. Madhavan, H.K. Babla, Xuan Hoang Le, Youqi Gang, B. Jäck, A. Gyenis, Nan Yao, R.J. Cava, N.P. de Leon, and A.A. Houck, New material platform for superconducting transmon qubits with coherence times exceeding 0.3 milliseconds, *Nat. Comm.* **12**, 1779 (2021).

[43] Chenlu Wang, Xuegang Li, Huikai Xu, Zhiyuan Li, Junhua Wang, Zhen Yang, Zhenyu Mi, Xuehui Liang, Tang Su, Chuhong Yang, Guangyue Wang, Wenyan Wang, Yongchao Li, Mo Chen, Chengyao Li, Kehuan Linghu, Jiaxiu Han, Yingshan Zhang, Yulong Feng, Yu Song, Teng Ma, Jingning Zhang, Ruixia Wang, Peng Zhao, Weiyang Liu, Guangming Xue, Yirong Jin, and Haifeng Yu, Towards practical quantum computers: transmon qubit with a lifetime approaching 0.5 milliseconds, *npj Quan. Inf.* **8**, 3 (2022).

[44] Xun-Wei Xu, Yanjun Zhao, Hui Wang, Aixi Chen, and Yu-Xi Liu, Nonreciprocal transition between two nondegenerate energy levels, *Photon. Res.* **9**, 87 (2021).

[45] Xun-Wei Xu, Yong Li, Baijun Li, Hui Jing, and Aixi Chen, Nonreciprocity via Nonlinearity and Synthetic Magnetism, *Phys. Rev. Applied* **13**, 044070 (2020).

[46] H. Ghaemi-Dizicheh, Transport effects in non-Hermitian nonreciprocal systems: General approach, *Phys. Rev. B* **107**, 125155 (2023).

[47] F. Roccati, G. Massimo Palma, F. Bagarello, and F. Ciccarello, Non-Hermitian physics and master equations, *Open Systems and Information Dynamics*, **29**, 2250004 (2022).

[48] F. Minganti, A. Miranowicz, R.W. Chhajlany, and F. Nori, Quantum exceptional points of non-Hermitian Hamiltonians and Liouvillians: The effects of quantum jumps, *Phys. Rev. A* **100**, 062131 (2019).

[49] X. Huang, C. Lu, C. Liang, H. Tao, and Y.-C. Liu, Loss induced nonreciprocity, *Light Sci. Appl.* **10**, 30 (2021).

[50] F. Roccati, S. Lorenzo, G. Calajò, G.M. Palma, A. Carollo, and F. Ciccarello, Exotic interactions mediated by a non-Hermitian photonic bath, *Optica* **9**, 565-571 (2022).

[51] F. Roccati, M. Bello, Zongping Gong, M. Ueda, F. Ciccarello, A. Chenu, and A. Carollo, F. Roccati, Hermitian and non-Hermitian topology from photon-mediated interactions, *Nat Commun* **15**, 2400 (2024).